

Potential and Current Density Distributions of Cranial Electrotherapy Stimulation (CES) in a Four-Concentric-Spheres Model

Mohammed Ferdjallah, *Member, IEEE*, Francis X. Bostick, Jr., and Ronald E. Barr,* *Member, IEEE*

Abstract—Cranial electrotherapy stimulation (CES) has been successfully used for treatment of many psychiatric diseases. Its noninvasive nature is its major advantage over other forms of treatments such as drugs. It is postulated that the low electric current of CES causes the release of neurotransmitters. However, the current pathways have not been extensively investigated. In the following paper, analytical and numerical methods are used to determine the distribution of potential and current density in a four zone concentric spheres model of the human head when excited by two electrodes diametrically opposite to each other. Because of the azimuthal symmetry, which is assumed in this study, a two-dimensional (2-D) finite difference approximation is derived in the spherical grid. The current density distribution is projected around the center of the model, where the thalamus is modeled as a concentric sphere. All dimensions and electrical properties of the model are adapted from clinical data. Results of this simulation indicate that, in contrast to previous beliefs, a small fraction of the CES current does reach the thalamic area and may facilitate the release of neurotransmitters.

I. INTRODUCTION

CRANIAL electrotherapy stimulation (CES) involves the application of a low electrical current to the human head through two circular electrodes placed behind the ears. CES has been successfully used for treatment of psychiatric diseases such as anxiety, depression, and insomnia [13], [18]. Its noninvasive nature is its major advantage over other forms of treatments such as drugs. Unlike electroconvulsive therapy (ECT), CES uses very low current magnitudes, and thus does not cause any memory loss or neuronal damage. Since its discovery, CES has been received with skepticism, since the applied low current, the low conductivity of the skull, and the high conductivity of the scalp, often lead one to believe all of the applied current will be dissipated on the surface of the scalp. Nevertheless, major effects have been observed during and after the administration of CES. CES was observed to cause sleep, relaxation, and well-developed alpha rhythm in the parietal-occipital cortex regions. The alpha activity is often correlated with the electrical activity of the thalamus, a deeper brain structure [3]. It is generally postulated that CES derives its treatment effects by stimulating brain

Manuscript received April 28, 1995; revised April 11, 1996. Asterisk indicates corresponding author.

M. Ferdjallah and F. X. Bostick, Jr. are with the Electrical Engineering Department and Biomedical Engineering Program, The University of Texas at Austin, Austin, TX 78712 USA.

*R. E. Barr is with the Mechanical Engineering Department, ETC 3.104A, The University of Texas at Austin, Austin, TX 78712 USA (e-mail: rbarr@mail.utexas.edu).

Publisher Item Identifier S 0018-9294(96)06110-1.

tissue to manufacture increased amounts of neurotransmitters, especially serotonin, beta endorphin, and norepinephrine [11], [14]. It is these observations which lead some researchers to believe that a fraction of the applied current eventually reaches the thalamus [15]. Consequently, the hypothesis that some CES current reaches deep brain structure is an attractive research proposition, and is the focus of this simulation study.

The current distribution in the brain has been the major concern of many investigators [4], [8], [12]. Brain researchers long have tried to correlate the current density distribution with biological behavior. Low-impedance electrodes with different configurations have been used to measure the current density with minimum distortion of the fields [8], [12]. A number of mathematical models have been used to estimate potential and current distributions, as well as the impedance of the different parts of the brain [7], [12].

In this paper, the potential field and the current density distributions are calculated when CES is applied to a four-zone concentric spheres model of the human head. These layers represent the brain, the cerebrospinal fluid, the skull, and the scalp. At the center of the model, the thalamus is modeled by a concentric sphere. The four-zone concentric spheres model is widely used and accepted for its quantitative agreement with a variety of general observations of the electroencephalogram (EEG) [9], [10]. The knowledge of the current density distribution inside the brain may assist CES researchers in choosing the proper injected current level to insure the effectiveness of CES therapy.

II. LAPLACE DIFFERENTIAL EQUATION: ANALYTICAL SOLUTION

A spherical model with four concentric shells is used for the human head. The brain tissue, the cerebrospinal fluid, the skull, and the scalp are represented by the four concentric zones with uniform conductivities (respectively, $\sigma_4, \sigma_3, \sigma_2$, and σ_1) and known outside radii (respectively, a_4, a_3, a_2 , and a_1) (Fig. 1). The conductivity of the scalp is assumed equal to that of the brain tissue. The electrical properties of the four layers of the model are adapted from clinical data [5]. The dimensions are measured from a magnetic resonance imaging (MRI) image of a 26-year-old Caucasian male. Time-varying current is applied through circular electrodes modeled as point sources and placed diametrically opposed to each other. For low-frequency time-varying fields, the wavelength of the harmonic fields is considerably larger than the dimensions of the average

human head. The conduction current is very large as compared to the displacement current. Consequently the displacement current terms are neglected. Also under these conditions, the time varying magnetic field has a negligible coupling to the electrical field, and thus induction terms are neglected. The electric field distribution at any time can be approximated by a static field satisfying the time-varying boundary conditions. The static potential distribution in the model is governed by Laplace's partial differential equation which can be written in spherical coordinates as

$$\frac{1}{r^2} \frac{\partial}{\partial r} \left(r^2 \frac{\partial V(t)}{\partial r} \right) + \frac{1}{r^2 \sin^2 \theta} \frac{\partial}{\partial \theta} \left(\sin^2 \theta \frac{\partial V(t)}{\partial \theta} \right) + \frac{1}{r^2 \sin^2 \theta} \frac{\partial^2 V(t)}{\partial \phi^2} = 0. \quad (1)$$

Because of the spherical geometry of the model, and assuming separation of variables, the general solution of Laplace's partial differential equation has the form [6]

$$V(r, \theta, \phi, t) = \rho(r)\Theta(\theta)\Xi(\phi)f(t) \quad (2)$$

where $f(t)$ is a time-varying function. For fields independent of ϕ , V may be written as a function of Legendre polynomials [2]

$$V(r, \theta, \phi, t) = f(t) \left[\sum_{n=0}^{\infty} A_n r^n P_n(\cos \theta) + \sum_{n=0}^{\infty} B_n r^{-(n+1)} P_n(\cos \theta) \right]. \quad (3)$$

The potential in the four-concentric-zone spherical model consists of four functions $V_1(t)$, $V_2(t)$, $V_3(t)$, and $V_4(t)$. In each zone the associated potential satisfies Laplace's equation in spherical coordinates and also satisfies the appropriate boundary conditions. These boundary conditions are as follows

$$\begin{aligned} -\sigma_1 \frac{\partial V_1(t)}{\partial r} &= I(r, \theta) & \text{at } r = a_1 \\ V_1(t) = V_2(t) & \text{ and } \sigma_1 \frac{\partial V_1(t)}{\partial r} = \sigma_2 \frac{\partial V_2(t)}{\partial r} & \text{at } r = a_2 \\ V_2(t) = V_3(t) & \text{ and } \sigma_2 \frac{\partial V_2(t)}{\partial r} = \sigma_3 \frac{\partial V_3(t)}{\partial r} & \text{at } r = a_3 \\ V_3(t) = V_4(t) & \text{ and } \sigma_3 \frac{\partial V_3(t)}{\partial r} = \sigma_4 \frac{\partial V_4(t)}{\partial r} & \text{at } r = a_4. \end{aligned} \quad (4)$$

Consider first the case of a sphere of uniform conductivity σ_1 and radius a_1 supplied by a current source ($+I(t)$) and a current sink ($-I(t)$) which are diametrically opposed to each other, the solution of Laplace's equation inside the sphere can be written as [16]

$$V(t) = \frac{I(t)}{2\pi\sigma_1} \sum_{n=1}^{\infty} \frac{(2n+1)}{2n} \frac{r^n}{a_1^{(n+1)}} P_n(\cos \theta). \quad (5)$$

Consider now the spherical model consisting of the four concentric spheres zones. The four zone potential functions $V_1(t)$, $V_2(t)$, $V_3(t)$, and $V_4(t)$ may be decomposed into a primary potential, which exists only when the sphere is made of a homogenous conductive material, plus secondary potentials due to the presence of layers of different conductivities. The

solutions for the different layers can be written as

$$V_1(t) = \frac{I(t)}{2\pi\sigma_1} \left[\Phi + \sum_{n=0}^{\infty} A_1(n)r^n P_n(\cos \theta) + \sum_{n=0}^{\infty} B_1(n)r^{-(n+1)} P_n(\cos \theta) \right] \quad (6a)$$

$$V_2(t) = \frac{I(t)}{2\pi\sigma_1} \left[\Phi + \sum_{n=0}^{\infty} A_2(n)r^n P_n(\cos \theta) + \sum_{n=0}^{\infty} B_2(n)r^{-(n+1)} P_n(\cos \theta) \right] \quad (6b)$$

$$V_3(t) = \frac{I(t)}{2\pi\sigma_1} \left[\Phi + \sum_{n=0}^{\infty} A_3(n)r^n P_n(\cos \theta) + \sum_{n=0}^{\infty} B_3(n)r^{-(n+1)} P_n(\cos \theta) \right] \quad (6c)$$

$$V_4(t) = \frac{I(t)}{2\pi\sigma_1} \left[\Phi + \sum_{n=0}^{\infty} A_4(n)r^n P_n(\cos \theta) + \sum_{n=0}^{\infty} B_4(n)r^{-(n+1)} P_n(\cos \theta) \right] \quad (6d)$$

where

$$\Phi = \sum_{n=1}^{\infty} \frac{(2n+1)}{2n} \frac{r^n}{a_1^{(n+1)}} P_n(\cos \theta) \quad (7)$$

is the primary potential and $A_i(n)$ and $B_i(n)$ are functions of n , which satisfy the boundary conditions of the model. The electrical current density is derived from the potential field solution. It is worthy to note that the analytical method is applied only to the spherical zoned model. Numerical methods, on the other hand, permit the conductive zones to be distorted away from the spherical geometry. As long as there is azimuthal symmetry the problem remains two dimensional (2-D). Even with azimuthal symmetry the layer shells of the model can be altered to closely resemble the human head.

III. FINITE DIFFERENCE APPROXIMATION

Kirchhoff's circuit laws are static approximations of Maxwell's equations and may be used as the basis for finite difference approximations [2]. Because of the spherical geometry of the model, polar coordinates (r, θ) are used in this study. The azimuthal symmetry eliminates the dependence on ϕ . The continuous circular medium is discretized by using a polar grid that divides the medium into a number of cells with irregular spacing in the r and θ directions. The coordinates (r, θ) are represented by (i, j) ($0 < i < m, 0 < j < n$), where the center of the circle ($r = 0, \theta = 0$) represents $(i = 0, j = 0)$. Laplace's equation at any interior node point (i, j) can be approximated by the finite difference equation as

$$\begin{aligned} [V(i, j) - V(i+1, j)]H(i, j) &+ [V(i, j) - V(i-1, j)]H(i-1, j) \\ + [V(i, j) - V(i, j+1)]G(i, j) &+ [V(i, j) - V(i, j-1)]G(i, j-1) = \frac{I(i, j)}{2\pi} \Delta\phi \end{aligned} \quad (8)$$

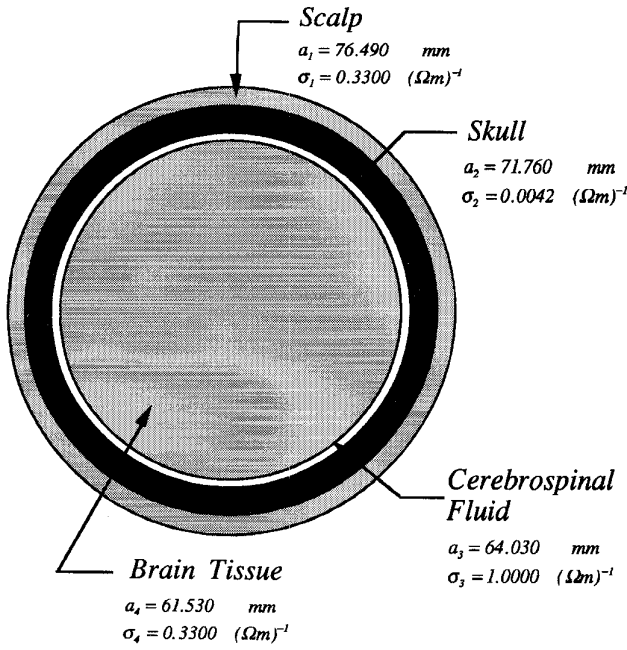


Fig. 1. The four concentric spheres model of the human head representing the brain tissue, the cerebrospinal fluid, the skull, and the scalp.

where $\Delta\phi$ is the length of the grid element in ϕ direction. The functions $H(i, j)$ and $G(i, j)$ are the conductances in r and θ directions

$$H(*, j) = \frac{[\sigma(*, j)\Delta S^N(*, j) + \sigma(*, j-1)\Delta S^S(*, j)]}{[r(*+1) - r(*)]} \quad (9a)$$

$$G(i, *) = \frac{[\sigma(i, *)\Delta A^E(i, *) + \sigma(i-1, *)\Delta A^W(i, *)]}{r(i)[\theta(*+1) - \theta(*)]} \quad (9b)$$

$\Delta S(i, j)$ and $\Delta A(i, j)$ are the surface elements crossed by the electrical field in the directions of the specified nodes, and are given by the following expressions

$$\Delta S^N(*, j) = \left[\frac{r(*) + r(*+1)}{2} \right]^2 \times \left[\cos[\theta(j)] - \cos\left[\frac{\theta(j+1) + \theta(j)}{2} \right] \right] \Delta\phi \quad (10a)$$

$$\Delta S^S(*, j) = \left[\frac{r(*) + r(*+1)}{2} \right]^2 \times \left[\cos\left[\frac{\theta(j-1) + \theta(j)}{2} \right] - \cos[\theta(j)] \right] \Delta\phi \quad (10b)$$

$$\Delta A^E(i, *) = \frac{1}{2} \left[\left[\frac{r(i+1) + r(i)}{2} \right]^2 - r^2(i) \right] \times \sin\left[\frac{\theta(*-1) + \theta(*)}{2} \right] \Delta\phi \quad (10c)$$

$$\Delta A^W(i, *) = \frac{1}{2} \left[r^2(i) - \left[\frac{r(i) + r(i-1)}{2} \right]^2 \right] \times \sin\left[\frac{\theta(*-1) + \theta(*)}{2} \right] \Delta\phi. \quad (10d)$$

The difference equation thus obtained indicates that the solution of the potential is dependent only on the adjacent values of the potential. The boundary condition between the different layers of the medium are satisfied across any spherical grid. While the difference equation (8) is valid only for interior nodes, it is somewhat altered to fit the boundary conditions. For the element (m, j) , where m is the maximum partition in the radial direction, one must have

$$H(m, j) = 0, \quad \text{and} \quad \Delta A^E(m, j) = 0 \quad \text{for } j = 1, 2, \dots, n. \quad (11)$$

The finite difference equation (8) on the surface of the sphere can be simplified to

$$\begin{aligned} & [V(m, j) - V(m-1, j)]H(m-1, j) \\ & + [V(m, j) - V(m, j+1)]G(i, j) \\ & + [V(m, j) - V(m, j-1)]G(m, j-1) = \frac{I(m, j)}{2\pi} \Delta\phi. \end{aligned} \quad (12)$$

The current density components are calculated by the following finite difference equations

$$J_r(i, j) = -\sigma(i, j) \frac{[V(i+1, j) - V(i-1, j)]}{[r(i+1) - r(i-1)]} \quad (13a)$$

$$J_\theta(i, j) = -\sigma(i, j) \frac{[V(i, j+1) - V(i, j-1)]}{r(i)[\theta(j+1) - \theta(j-1)]}. \quad (13b)$$

IV. APPLICATION

The four-concentric-spheres model of the human head is excited by a pair of electrodes placed diametrically opposed to each other. The electrodes are placed diametrically opposite to each other not only to mimic CES application, but also to maximize the penetrating current density. The potential distribution calculated, for 1-mA input current, by the analytical solution compares very well to that calculated by the numerical solution at the exception of the vicinity of the source (Fig. 2), where the numerical solution underestimates the potential field. The potential field for various angles away from the point source exhibits plateaus in the scalp and the skull areas due to the large gradient in conductivity. Although the potential field drops drastically beyond one tenth of the total radius from the surface of the sphere, it remains relatively constant in the brain tissue layer. Consequently, the potential distribution map shows equipotential lines which segregate mainly around the electrodes (Fig. 3). The equipotential lines are relatively parallel and concentric in the brain tissue layer.

The radial current density is calculated at $\theta = 0$, and plotted as a function of the radius (Fig. 4). The tangential current density at $\theta = 0$ is equal to zero due to the symmetry of the model. Consequently, the tangential current density is calculated near the stimulating electrode (assumed to be a point source) at $\theta = \pi/2N$, where N is the number of partitions in the θ direction. The tangential current density is also plotted as a function of the radius (Fig. 5). The tangential current density component indicates clearly the discontinuity of the conductivity of the medium. The radial current density distribution drops to 0.001% at a radius of 13.30 mm (an average radius for the thalamus which is estimated from the

TABLE I

	$ J_r(r, \theta=0) $ ($\mu\text{A}/\text{cm}^2$)	$ J_\theta(r, \theta=\pi/2N) $ $N=100$ ($\mu\text{A}/\text{cm}^2$)	$ E $ (V/m)
Scalp (76.49mm)	3×10^5	1×10^6	3×10^6
Skull (71.76mm)	30	2×10^{-1}	70
Cerebrospinal Fluid (64.03mm)	15	7×10^{-2}	0.15
Brain Tissue (61.53mm)	10	2×10^{-2}	0.3
Thalamus (13.30mm)	5	5×10^{-3}	0.15

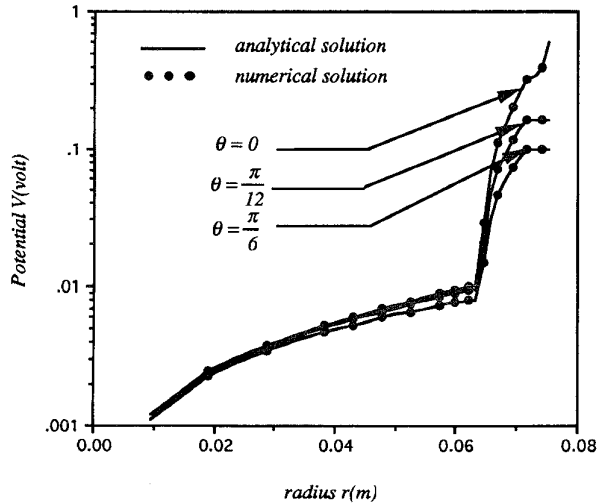


Fig. 2. The numerical solution (dotted line) versus the analytical solution of the potential distribution $V(r, \theta)$ as function of the radius for certain angle values.

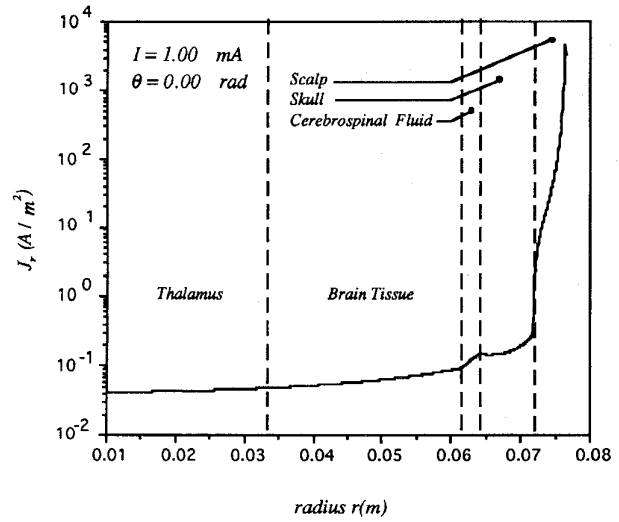


Fig. 4. The radial current density distribution $J_r(r, \theta)$ at $\theta = 0$, as a function of the radius.

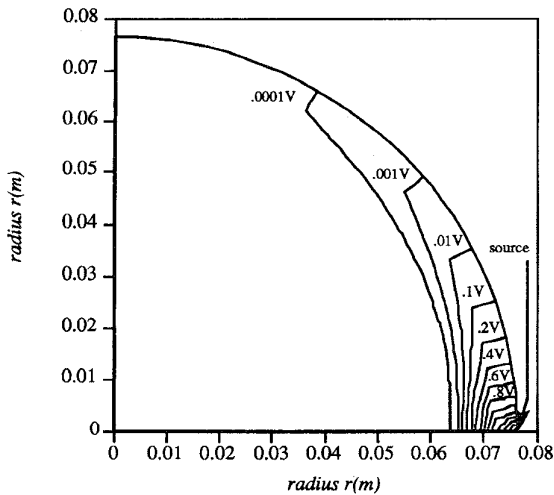


Fig. 3. Mapping of the potential distribution $V(r, \theta)$.

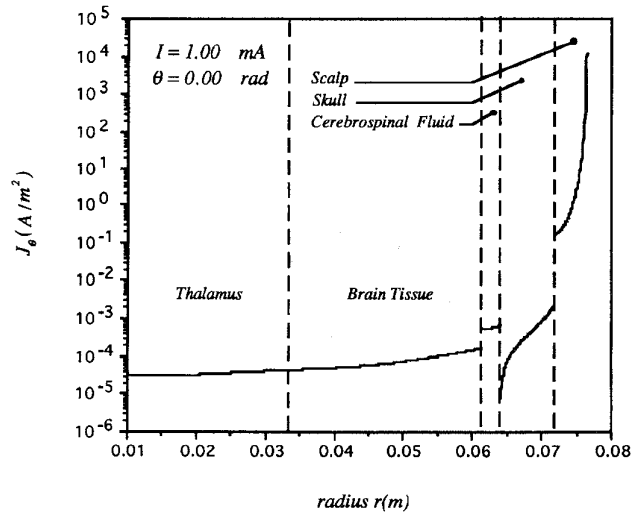


Fig. 5. The tangential current density distribution $J_\theta(r, \theta)$ at $\theta = \pi/2N$ ($N = 100$), as a function of the radius.

same subject's MRI image). The tangential current density shows a plateau for radii less than 60.0 mm. Most of the current flows near the surface of the model. At the surface of the brain tissue layer the radial current density drops to 0.003% while the tangential current density drops to 0.000 001% (Table I). Consequently, most of the current which penetrates the model is conducted radially.

V. DISCUSSION AND CONCLUSION

The potential and the current density distributions were calculated by two different methods. Although the analytical solution is accurate, the numerical solution is often preferred over the analytical method to accommodate variations in the resistivity distribution of the layers of the model. The

numerical method established in this study through the use of a resistivity model simplifies the three dimensional spherical domain to a 2-D polar coordinate problem.

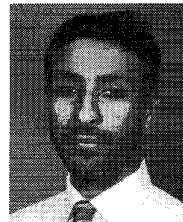
The radial current density is more appreciable than that of the tangential current density distribution. Based on this simulation, the maximum injected current density by the CES therapy, using a standard 1-mA stimulus, is about $5 \mu\text{A}/\text{cm}^2$ at a radius of 13.30 mm (thalamic area) of the model. This demonstrates that some portion of the stimulating current does reach deep brain structure. Although the current density needed to elicit a functional response is larger than $300 \mu\text{A}/\text{cm}^2$ [17], CES as a facilitating stimulus is still plausible because the electrical field lines are parallel to the neuronal structure of the brain. The physiological effect of CES may not be specific, nonetheless the amount of current density which reaches the brain may cause the release of neurotransmitters which in turn cause physiological effects such as relaxation.

The electrical field computed at the surface of the thalamus is about 0.15 V/m. In general and throughout the brain tissue the electrical field (outside the neuron cell) is about eight times that caused by thermal noise (0.02 V/m). However, this computed electrical field as compared to that of the thermal noise inside the neuron cell (500 V/m) is very low and may not cause any physiological effects on the neuron cell [1]. Nonetheless, the CES electrical field as a facilitating stimulus could cause the release of neurotransmitters responsible for physiological effects.

A future modification of the electrode setup for cranial electrical stimulation (CES) calls for the use of multiple electrodes for injecting current. The use of multiple electrodes increases the amount of current penetrating the brain tissue, and allows the possibility of exciting different parts of the brain that are of interest to a specific treatment. A more precise model for the human head is needed to accurately predict the current density distribution and to take into consideration the variation in the dimensions as well as in the electrical properties of the different compartments of the head.

REFERENCES

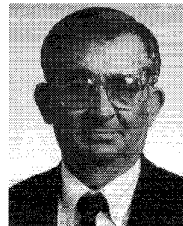
- [1] K. R. Adair, "Constraints on biological effects of weak extremely-low-frequency electromagnetic fields," *Physical Rev.*, vol. 43, no. 2, pp. 1039-1048, 1991.
- [2] K. L. Binns, P. J. Lawrenson, and C. W. Trowbridge, *The Analytical and Numerical Solutions of Electric and Magnetic Fields*. New York: Wiley, 1992.
- [3] A. Childs and M. Crismon, "The use of cranial electrotherapy stimulation in post-traumatic amnesia: A report of two cases," *Brain Injury*, vol. 2, no. 3, pp. 243-247, 1988.
- [4] A. M. Dymon, R. W. Coger, and E. A. Serafetinides, "Intracerebral current levels in man during electrosleep therapy," *Biological Psych.*, vol. 10, pp. 101-104, 1975.
- [5] L. A. Geddes and L. E. Baker, "The specific resistance of biological materials: A compendium of data for the biomedical engineer and physiologist," *Med., Biol. Eng.*, vol. 5, pp. 271-293, 1967.
- [6] L. D. Landau and E. M. Lifshitz, *Electrodynamics of Continuous Media*, Elmsford, NY: Pergamon, 1960.
- [7] D. Murphy, P. Burton, R. Coombs, L. Tarassenko, and P. Rolfe, "Impedance imaging in the newborn," *Clin. Phys. Physiological Meas.*, vol. 8, Suppl. A, pp. 131-140, 1987.
- [8] J. B. Myklebust, J. F. Cusick, A. Sances, Jr., and S. J. Larson, *Neural Stimulation*, Vols. 1, 2. Boca Raton, FL, 1985.
- [9] P. L. Nunez, *Electric Fields of the Brain*. New York: Oxford University Press, 1981.
- [10] P. L. Nunez, "Removal of reference electrode and volume conduction effects by spatial deconvolution of evoked potentials using a three concentric sphere model of the head," in *Proc. London Symp., Electroencephalogr., Clin. Neurophysiol.*, 1987, vol. 39, Suppl., pp. 143-148.
- [11] E. G. Peniston and P. J. Kulkosky, " α - θ brainwave training and β -endorphin levels in alcoholics," *Alcoholism: Clin., Experimental Res.*, vol. 13-2, pp. 271-279, 1989.
- [12] S. Ruch and D. Driscoll, "Current distribution in the brain from surface electrodes," *Anesth., Analgesia*, vol. 47, pp. 717-723, 1968.
- [13] R. Schmitt, T. Capo, and E. Boyd, "Cranial electrotherapy stimulation treatment for anxiety in chemically dependent persons," *Alcoholism: Clin., Experimental Res.*, vol. 10, no. 2, pp. 158-160, 1986.
- [14] C. Shealy, R. Cady, R. Wilkie, R. Cox, S. Liss, and W. Clossen, "Depression—A diagnostic, neurochemical profile and therapy with cranial electrical stimulation (CES)," *J. Neurological, Orthopedic Med., Surg.*, vol. 10, no. 4, pp. 301-303, 1989.
- [15] R. B. Smith, "The effects of cerebral electrotherapy on short-term memory impairment in alcoholic patients," *Int. J. Addictions*, vol. 12, no. 4, pp. 575-582, 1977.
- [16] A. N. Tikhonov and A. A. Samarskii, *Equations of Mathematical Physics*. New York: Macmillan, 1963.
- [17] J. S. Yeomans, *Principles of Brain Stimulation*. New York: Oxford University Press, 1990.
- [18] M. F. Weiss, "The treatment of insomnia through the use of electrosleep: An EEG study," *J. Nervous and Mental Diseases*, vol. 157, pp. 108-120, 1973.



Mohammed Ferdjallah (M'95) received the bachelors degree in electronics from Ecole National Polytechnique, Algiers, Algeria, in 1985, and both the masters degree in biomedical engineering and Ph.D. degree in electrical and computer engineering, from The University of Texas at Austin in 1988, and 1994, respectively. Currently, he is an National Institutes of Health (NIH) postdoctoral fellow at the Medical College of Wisconsin, Milwaukee.

His research interests include adaptive signal processing, biosignal processing, bioelectromagnetics, neural electrical stimulation, multichannel EMG processing, fiber optics sensors, and instrumentation.

Dr. Ferdjallah received a student paper award at the 30th Annual Rocky Mountain Bioengineering Symposium in 1993.



Francis X. Bostick Jr. received the B.S., M.S., and Ph.D. degrees in electrical engineering from The University of Texas at Austin in 1955, 1961, and 1964, respectively.

He was a Research Engineer with the Electrical Engineering Research Laboratory at UT Austin from 1955 until 1963 when he joined the faculty of the Electrical and Computer Engineering Department. He is currently a professor there and teaches courses in electromagnetics and electrical geophysics. He maintains an active research effort in both surface electrical exploration methods and in electrical well logging.



Ronald E. Barr (S'75-M'75) received both the B.S.E.E. and Ph.D. degrees from Marquette University, Milwaukee, WI, in 1969 and 1975, respectively.

He is currently Professor of Mechanical and Biomedical Engineering at The University of Texas at Austin, where he has taught since 1978. He previously taught at Texas A&M University, College Station, from 1975-1978. His research interests include biosignal analysis, biomechanics of human movement, and engineering computer graphics.

Dr. Barr is a registered Professional Engineer (PE) in the state of Texas. He has received the AT&T Foundation Award for Excellence in Engineering Teaching (1990) and the ASEE Chester F. Carlson Award for Innovation in Engineering Education (1993).